

**OPEN ACCESS**

# Isoxazole-Based Electrolytes for Lithium Metal Protection and Lithium-Sulfurized Polyacrylonitrile (SPAN) Battery Operating at Low Temperature

To cite this article: Sha Tan *et al* 2022 *J. Electrochem. Soc.* **169** 030513

View the [article online](#) for updates and enhancements.



The Electrochemical Society  
Advancing solid state & electrochemical science & technology

242nd ECS Meeting

Oct 9 – 13, 2022 • Atlanta, GA, US

Abstract submission deadline: **April 8, 2022**

Connect. Engage. Champion. Empower. Accelerate.

**MOVE SCIENCE FORWARD**



Submit your abstract





# Isoxazole-Based Electrolytes for Lithium Metal Protection and Lithium-Sulfurized Polyacrylonitrile (SPAN) Battery Operating at Low Temperature

Sha Tan,<sup>1</sup> Haodong Liu,<sup>2</sup> Zhaohui Wu,<sup>2</sup> Conan Weiland,<sup>3</sup> Seong-Min Bak,<sup>4</sup> Arthur Ronne,<sup>1</sup> Ping Liu,<sup>2</sup> M. Stanley Whittingham,<sup>5</sup> Zulipiya Shadike,<sup>1,z</sup> Enyuan Hu,<sup>1,z</sup> and Xiao-Qing Yang<sup>1,z</sup>

<sup>1</sup>Chemistry Division, Brookhaven National Laboratory, Upton, NY, 11973, United States of America

<sup>2</sup>Department of Nano Engineering, University of California San Diego, La Jolla, CA, 92093, United States of America

<sup>3</sup>Material Measurement Laboratory, National Institute of Standards and Technology, Gaithersburg, MD 20899, United States of America

<sup>4</sup>National Synchrotron Light Source II, Brookhaven National Laboratory, Upton, NY, 11973, United States of America

<sup>5</sup>Materials Science and Engineering Program, Binghamton University, Binghamton, NY, 13902, United States of America

A new electrolyte system using isoxazole as the salt dissolving solvent has been developed and studied for lithium metal batteries. By using fluoroethylene carbonate (FEC) as an additive and 1,1,2,2-tetrafluoroethyl-2,2,3,3-tetrafluoropropyl ether (TTE) as a diluent for localized high concentration electrolyte (LHCE), isoxazole-based electrolytes were successfully implemented in lithium metal batteries, demonstrating excellent lithium metal protection capability. Utilizing several advanced characterization techniques (including synchrotron-based X-ray absorption spectroscopy and photoelectron spectroscopy), the solid electrolyte interphase (SEI) formed on the Li-metal anode after employing these electrolytes was thoroughly investigated. The high ionic conductivity of isoxazole at low temperature and the low impedance of SEI formed in LHCE significantly improved the low-temperature performance of Li-sulfurized polyacrylonitrile (SPAN) batteries, delivering 273.8 mAh g<sup>-1</sup> capacity at -30 °C with 99.85% capacity retention after 50 cycles.

© 2022 The Author(s). Published on behalf of The Electrochemical Society by IOP Publishing Limited. This is an open access article distributed under the terms of the Creative Commons Attribution 4.0 License (CC BY, <http://creativecommons.org/licenses/by/4.0/>), which permits unrestricted reuse of the work in any medium, provided the original work is properly cited. [DOI: 10.1149/1945-7111/ac58c5]



Manuscript submitted December 12, 2021; revised manuscript received January 31, 2022. Published March 7, 2022. *This paper is part of the JES Focus Issue on Focus Issue In Honor of John Goodenough: A Centenarian Milestone.*

For the research and development of the rechargeable lithium-ion and lithium metal battery systems, electrolyte engineering has been recognized as a critically important part of ensuring stable cell operation.<sup>1-6</sup> During the formation cycles, insoluble electrolyte decomposition products deposit on the electrodes, forming solid electrolyte interphase (SEI) on the anode and cathode electrolyte interphase (CEI) on the cathode. These interphases passivate the electrodes and prevent further electrolyte decomposition. In addition to the critical role of contributing to interphase protective capability, the ionic conductivity of electrolyte also needs to be considered, which directly determines the battery kinetics and affects fast charging capability and low temperature performance.

Most of the electrolyte engineering studies have been focusing on electrolyte formulation by optimizing the salts, solvents, additives, and their combinations, especially the development of additives for improving interphasial properties.<sup>7,8</sup> Recently, it has been reported that changing electrolyte concentration is a very effective approach, which can alter the solvation structure and change the interphasial properties. Zhang's group<sup>9-11</sup> designed several high concentration electrolytes (HCE) and localized high concentration electrolytes (LHCE), demonstrating highly enhanced Li metal passivation as well as high voltage cathode protection.

Since most of these studies have been focused on using two types of electrolyte solvents, carbonates and ethers, exploring different types of novel solvents and studying their electrochemical properties will open new approaches for future electrolyte designs. Our previous work identified a highly promising electrolyte solvent, isoxazole (IZ),<sup>12,13</sup> which has high ionic conductivity and a low melting point. Electrolytes using IZ demonstrated considerably improved low-temperature performance of Li/graphite cells. In this work, the stability of IZ for lithium metal batteries (LMB) is systematically studied. Four different IZ-based electrolytes were prepared, including two LHCE electrolytes with different solvent/

diluent volume ratios, where IZ was used as an electrolyte solvent and 1,1,2,2-tetrafluoroethyl-2,2,3,3-tetrafluoropropyl ether (TTE) was used as a diluent (in the rest part of this paper, all the LHCE are referred to this formulation with IZ:TTE volume ratio of 1:3 as LHCE-TTE3 and 1:4.5 as LHCE-TTE4.5). The molecular structures of the Lithium bis(fluorosulfonyl)imide (LiFSI) salt, IZ solvent, FEC additive, and TTE diluent are shown in Fig. 1. Compared with 1 M LiFSI-IZ electrolytes without TTE diluent, both LHCEs exhibited considerably improved SEI passivation ability. The effects of using different IZ/TTE volume ratios were also studied. Better performances of Li-Li, Li-Cu, and Li-SPAN cells were obtained when using LHCE with a lower IZ ratio, which had more FSI<sup>-</sup> in solvation structure and mainly formed anion derived SEI with sulfur-species-rich and F-rich components. At low temperatures, Li-SPAN batteries using LHCE-TTE4.5 electrolyte with lower IZ/TTE ratio demonstrated superior performance than the LHCE-TTE3. Benefitted from the more stable SEI formed in LHCE electrolyte, the Li/SPAN cell using LHCE-TTE4.5 delivered 340.7 mAh g<sup>-1</sup> at -20 °C and 273.8 mAh g<sup>-1</sup> at -30 °C respectively with 99.85% capacity retention after 50 cycles at -30 °C. This is much better than the higher IZ:TTE ratio LHCE-TTE3 electrolyte. In contrast, as reported before,<sup>14</sup> the capacity of the cell using baseline electrolyte of 1 M LiFSI in 1,3-dioxolane/1,2-dimethoxyethane (DOL/DME) dropped significantly at low temperature.

## Experimental

**Electrolyte and electrode preparations.**—Battery grade lithium bis(fluorosulfonyl)imide (LiFSI), IZ, FEC, and TTE were used. The electrolytes were made by dissolving LiFSI in IZ or IZ/TTE mixtures inside an Ar-filled glove box. Specifically, 1 M LiFSI in IZ, 1 M LiFSI in IZ with 10% vol. FEC, 1 M LiFSI in IZ/TTE (volume ratio: 1: 3) with 10 vol% FEC, and 1 M LiFSI in IZ/TTE (volume ratio: 1: 4.5) with 10 vol% FEC were prepared. For SPAN electrodes, the SPAN slurry was prepared by mixing active material (SPAN powder, 80 wt%), conducting agent (super P carbon, 10 wt%) and binder (Polyvinylidene fluoride, PVDF, 10 wt%), then

<sup>z</sup>E-mail: zshadike@sju.edu.cn; enhu@bnl.gov; xyang@bnl.gov

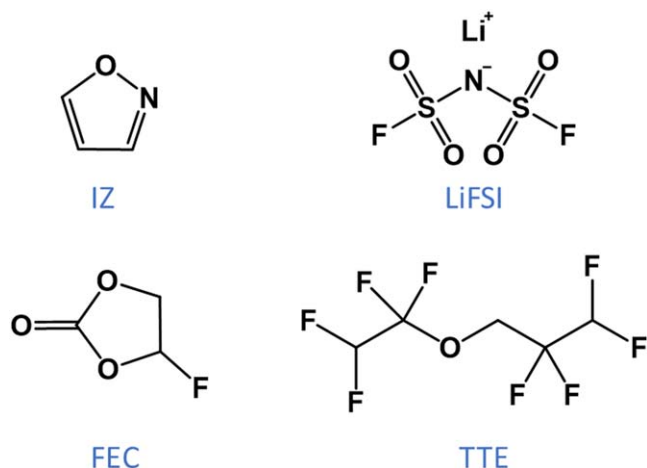


**Figure 1.** Structures of isoxazole (IZ); Lithium bis(fluorosulfonyl)imide (LiFSI); Fluoroethylene carbonate (FEC); 1, 1, 2, 2-tetrafluoroethyl-2, 2, 3, 3-tetrafluoropropyl ether (TTE).

dispersing the mixture by N-methyl-2-pyrrolidone (NMP) to make a slurry. Afterward, the slurry was uniformly coated onto Al foil and vacuum dried at 80 °C overnight. The dried SPAN electrodes were punched into ½ inch diameter discs with an active material mass loading of ~4 mg.

**Electrochemical measurements.**—Li/Cu cells were assembled using Li foil and Cu foil and tested following method 2 in Zhang's work to measure the Li metal's coulombic efficiency (CE).<sup>15</sup> The total charge ( $Q_t$ ) was 5 mAh cm<sup>-2</sup>, cycled charge ( $Q_c$ ) was 1 mAh cm<sup>-2</sup> and cycled number was 10. After obtaining the final stripping capacity ( $Q_s$ ), CE was calculated using the equation below:

$$CE = \frac{nQ_c + Q_s}{nQ_c + Q_t}$$

The cycling performance of Li/Li symmetric cell was measured at a current density of 1 mA cm<sup>-2</sup> with a stripping/plating capacity of 1 mAh cm<sup>-2</sup>. The galvanostatic charge/discharge curves of Li/SPAN cells were tested using a Neware battery cycler. The 2032-type coin cells were assembled inside an Ar-filled glove box using a polypropylene (Celgard 3501) as separator. The Li/SPAN cells were cycled between 1.0 ~ 3.0 V, using a current density of 0.1 A g<sup>-1</sup>. Li/SPAN cells were activated at room temperature at 0.05 A g<sup>-1</sup> for two cycles to stabilize interphases for the low-temperature electrochemical performance test. Afterward, charge/discharge performance at -20 °C and -30 °C were tested using MTI battery cycler and Tenney environment chamber. The Li/Cu, Li/Li and Li/SPAN coin cells mentioned above used 70 μl electrolyte for electrochemical characterizations. The impedance of the low temperature cycled cell was tested using an impedance analyzer (BioLogic SAS) at the open circuit voltage in a frequency range from 100 mHZ to ~1 MHz to collect electrochemical impedance spectroscopy (EIS) data.

For measuring ionic conductivity, EIS was conducted using symmetric cells with two platinum electrodes symmetrically placed in the electrolyte solution. After collecting EIS spectra via an impedance analyzer (BioLogic SAS) at the open circuit voltage and a 1 HZ ~ 100 kHz frequency range, at controlled temperatures using Tenney environment chamber, solution resistance at various temperatures was obtained, and it can be converted to ionic conductivity following the equation:<sup>16</sup> The reciprocal of resistivity ( $\rho$ ) is the ionic conductivity.

$$R = \rho \frac{l}{A}$$

Where  $l$  is the distance between the electrodes,  $A$  is the Pt electrode area,  $R$  represents solution resistance, and  $\rho$  is the resistivity. To obtain the  $l$  and  $A$  constant of the cell, a standard solution of 1 wt% KCl was used.

**Scanning electron microscopy (SEM), X-ray fluorescence (XRF) imaging, X-ray absorption spectroscopy (XAS), and hard X-ray photoemission spectroscopy (HAXPES) characterizations.**—To study the morphology of deposited Li, 1.0 mAh cm<sup>-2</sup> of lithium was deposited on Cu foil at a current density of 1.0 mA cm<sup>-2</sup> in Li/Cu cells after 10 cycles. Then, cells were disassembled, after washing and drying, the harvested Cu foils were mounted onto a SEM holder and imaged using a Hitachi SEM 4800 at the Center for Functional Nanomaterials (CFN) of the Brookhaven National Laboratory (BNL). The XRF imaging and Sulfur K-edge XAS data were collected at the 8-BM (TES) beamline of the National Synchrotron Light Source II (NSLS II) of BNL. Before the synchrotron characterization, the cycled Cu foils in Li/Cu cells were collected, washed, and dried, then cut into 5 × 5 mm<sup>2</sup> pieces, sealed between Kapton tape and polypropylene thin film then mounted onto the sample holders. The HAXPES measurement was carried out at beamline 7-ID-2 of NSLS II at BNL. Samples were transferred to the beamline under Argon gas and introduced into the vacuum chamber to minimize exposure to air. The Li foil collected from cycled SPAN cells were mounted onto sample holder after washing and drying. Photon energy selection was obtained using a double-crystal monochromator. Measurements were made with a 400 mm diameter hemispherical electron analyzer mounted perpendicular to the photon propagation direction and parallel to the electric polarization direction.

## Results and Discussion

Four different IZ-based electrolytes were studied to understand the compatibility of IZ for Li metal and Li-SPAN system. Formulations of electrolytes are 1 M LiFSI in IZ (denoted as EIZ), 1 M LiFSI in IZ with 10% FEC (denoted as EIZ-FEC), 1 M LiFSI in isoxazole/TTE (volume ratio: 1: 3) with 10% FEC (denoted as LHCE-TTE3), and 1 M LiFSI in isoxazole/TTE (volume ratio: 1: 4.5) with 10% FEC (denoted as LHCE-TTE4.5), respectively. The reason for choosing volume ratios of 1:3 and 1:4.5 is based on the limited solubility of LiFSI in isoxazole. Because diluent is not able to dissociate salts, if the amount of diluent were increased further (more than 4.5), the salt would not be fully dissolved and precipitated salt would be observed after storage. Li/Li symmetric cell cycling performance was tested at a current density of 1 mA cm<sup>-2</sup> with an areal capacity of 1 mAh cm<sup>-2</sup>, and results are shown in Fig. 2a. Because of the instability between IZ and Li anode, the Li/Li cells using EIZ electrolyte suffered fast overpotential build-up and cell shortening after ~16 h. However, when 10% FEC additive was introduced to the electrolyte, Li/Li cell life span was successfully extended to ~270 h with small overpotential during cycling. This could be ascribed to the FEC-generated SEI. To further improve the cyclability of LMB and the stability between solvent and Li metal, LHCE, which has been identified as an effective way by providing low viscosity, low cost, and ability to form anion derived SEI to passivate and protect Li metal anode, was further studied. Herein, two LHCE systems with different solvent/diluent ratios, LHCE-TTE3 and LHCE-TTE4.5 were prepared. In Fig. 2a, compared to the EIZ and EIZ-FEC, more stable overpotentials were observed for Li/Li cells using LHCE-TTE3 and LHCE-TTE4.5, indicating that stable SEI formed on lithium metal anode (LMA) in LHCE. The improved interphase protection also enabled a longer cycling life, especially for cells using LHCE-TTE4.5. The Li/Li cell cycled for more than 450 h without short-

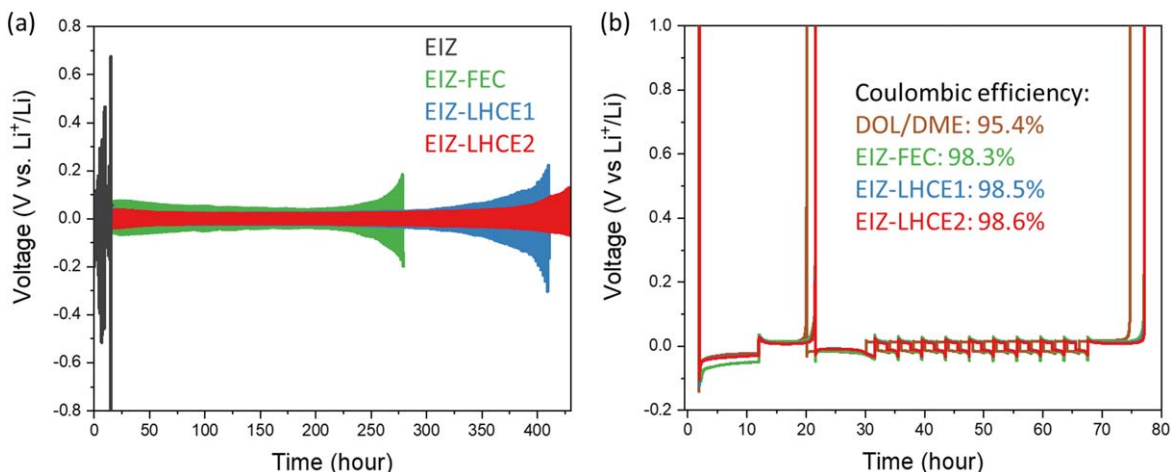


**Figure 2.** (a) Electrochemical performances of Li/Li symmetric cells using different isoxazole-based electrolytes; (b) Coulombic efficiency of Li/Cu cells and the voltage profiles.

circuiting. Figure 2b shows the voltage profiles of the Li/Cu cells used for CE evaluation using the protocol proposed by Zhang et al.<sup>15</sup> with details in the experimental section. Among these four different electrolytes, LHCEs showed CEs of 98.5% for LHCE-TTE3 and 98.6% for LHCE-TTE4.5, both are higher than that of EIZ-FEC (98.3%) and the ether electrolyte (1 M LiTFSI in DOL/DME) (95.4%). These values are much higher than the reported CE (89.8%) for the conventional electrolyte using 1 M LiPF<sub>6</sub> in EC-EMC with 2% vinylene carbonate (VC) tested under the same condition.<sup>17</sup> It is worth pointing out that most of the LiFSI salts were dissociated only in IZ due to the limited salt solubility of TTE. Therefore, with a smaller IZ amount in LHCE-TTE4.5, there should be more FSI<sup>-</sup> anions inside the solvation shell, and thus more anion derived species could be generated to form a better SEI leading to a better electrochemical performance. According to the electrochemical performance of the Li/Li and Li/Cu cells, better Li metal passivation was achieved using LHCEs. Further interphase characterizations were carried out on the cycled Li/Cu cells to have a better understanding of the effects of this solvent/diluent ratio on electrochemical performances. The deposited lithium morphology (top view and cross section view) was imaged using SEM. Loose deposited Li and cracks of the deposited Li was observed using baseline DOL/DME electrolyte (Figs. 3a and 3b). Compared with the deposited Li using LHCE-TTE3 electrolyte (Figs. 3c and 3d), which also show cracks and loose contact with Cu substrate, quite different morphology was observed for cells using LHCE-TTE4.5 electrolyte (Figs. 3e and 3f): Large granular particles with much denser and compact deposited Li were observed. This could result in less side reactions with electrolyte, and eventually higher CE,<sup>18</sup> due to decreased surface area.

It has been reported in the literature that in LHCE electrolytes, the lowest unoccupied molecular orbital (LUMO) is shifted to the anion, generating an anion-derived interphase.<sup>19</sup> Sulfur is the unique element in FSI<sup>-</sup> only, not in any of the solvents. Therefore, sulfur K-edge XAS was carried out to identify the composition of the sulfur species from FSI<sup>-</sup> reduction in the interphase of cycled Li/Cu cells. As shown in Fig. 4a, FSI anions were decomposed in both LHCE-TTE3 and LHCE-TTE4.5 electrolytes, generating Li<sub>2</sub>S, SO<sub>3</sub><sup>2-</sup>, and COSO<sub>2</sub><sup>-</sup> species with similar intensity distribution. X-ray fluorescence (XRF) imaging was performed with an incident photon energy at 2482 eV to investigate the spatial distribution of sulfur species. As shown in Figs. 4b and 4c, relative homogenous sulfur species distribution was observed in both systems, indicating homogenous FSI<sup>-</sup> derived interphase formation. Higher sulfur signal intensity in Fig. 4c suggests more sulfur species in the interphase when using LHCE-TTE4.5 electrolyte, which is attributed to more anions located inside the solvation structure due to lower IZ amount in

LHCE-TTE4.5, resulting in more FSI<sup>-</sup> decomposition species and better SEI for Li metal passivation. Therefore, compared with the solvent derived SEI generated inside DOL/DME, which is consisting of organic species (i.e., poly(DOL), alkoxides, etc),<sup>20,21</sup> SEI formed by anion reduction inside LHCEs provided better Li metal passivation, enabling uniform and dense Li deposition and higher CE.

The electrochemical performance of Li/SPAN full cells were tested using IZ electrolytes. There are two reasons for choosing SPAN as the cathode for this study. One is the limited oxidation stability of IZ at high voltage charging restricted its application for high voltage transition metal oxide cathodes, while it is not a problem for the low voltage sulfur cathodes. Another reason is based on the desirable properties of SPAN cathode, which has higher reversible capacity with high sulfur utilization and stable cycling life comparing with elemental sulfur in Li-S batteries. Commonly used 1 M LiTFSI in DOL/DME electrolyte was used as a baseline for comparison. Although DOL/DME enables better Li metal protection, as shown in Fig. 5a, the instability between the SPAN cathode and ether electrolytes leads to fast capacity decay, similar as reported in the literature.<sup>14,22</sup> In contrast, LHCE electrolytes have a more stable capacity retention (Figs. 5b and 5c), due to their good Li metal anode protection as well as stability with the SPAN cathode. Figure 5d depicts the long-term cycling capacity retention and high CE of Li/SPAN cells, further indicating the superior performance of LHCE electrolytes.

To investigate the SEI composition in the cycled Li-SPAN cell, HAXPES studies using two photon energies (2000 eV, 6000 eV) were conducted to understand the distribution of electrolyte decomposition products at different penetration depths. The results are summarized in Fig. 6. The top two rows presented the collected XPS spectra at 2000 eV, corresponding to the SEI top layer. Moreover, the bottom two rows were measured at 6000 eV, showing the SEI inner layer compositions. Comparing S 2p spectra at 2000 eV, the outer layers generated in both electrolytes consisted of similar components, in good agreement with sulfur XAS results. A large amount of SO<sub>2</sub>F and SO<sub>x</sub> species, corresponding to FSI<sup>-</sup> reduction in LHCEs, suggested formation of FSI<sup>-</sup> derived SEI components rather than the solvent decomposition. In addition, another decomposition product of FSI<sup>-</sup> anions, not of the solvents, LiF, was also observed on the outer layer in large quantities. When the photon energy was increased to 6000 eV in probing the inner layer, the sulfur species signal was significantly decreased, as well as the N signals, suggesting that less FSI reduction products and less IZ decomposition products exist in the bottom layer. At the same time, a large amounts of Li<sub>2</sub>O and LiF were observed, which might be attributed more to the decomposition of the FEC additive and less to the FSI<sup>-</sup> anion. In summary, for both LHCE-TTE3 and LHCE-

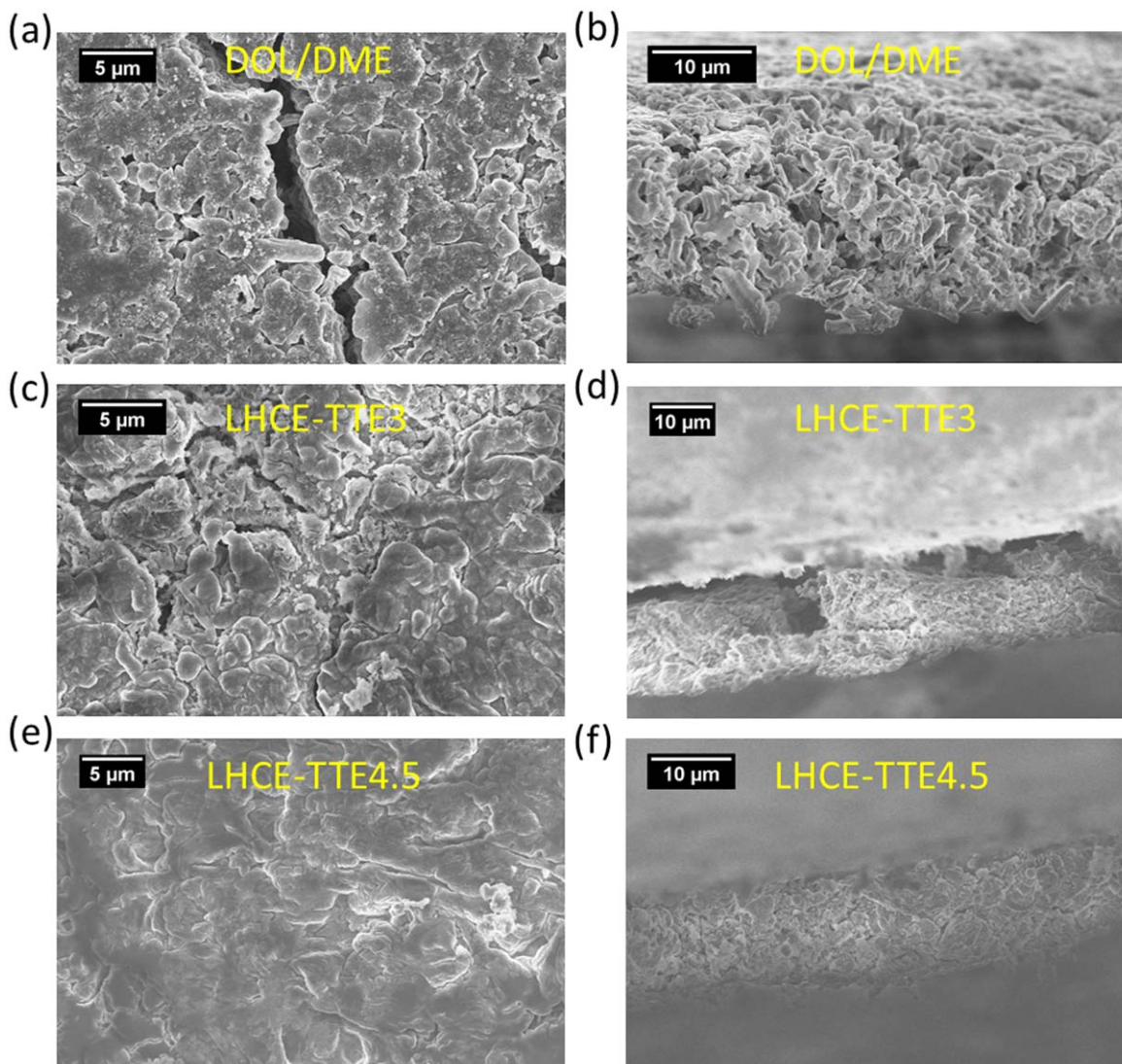


**Figure 3.** SEM images of deposited lithium on Cu foil in Li/Cu cells using (a)–(b) 1 M LiTFSI in DOL/DME, (c)–(d) LHCE-TTE3, (e)–(f) LHCE-TTE4.5.

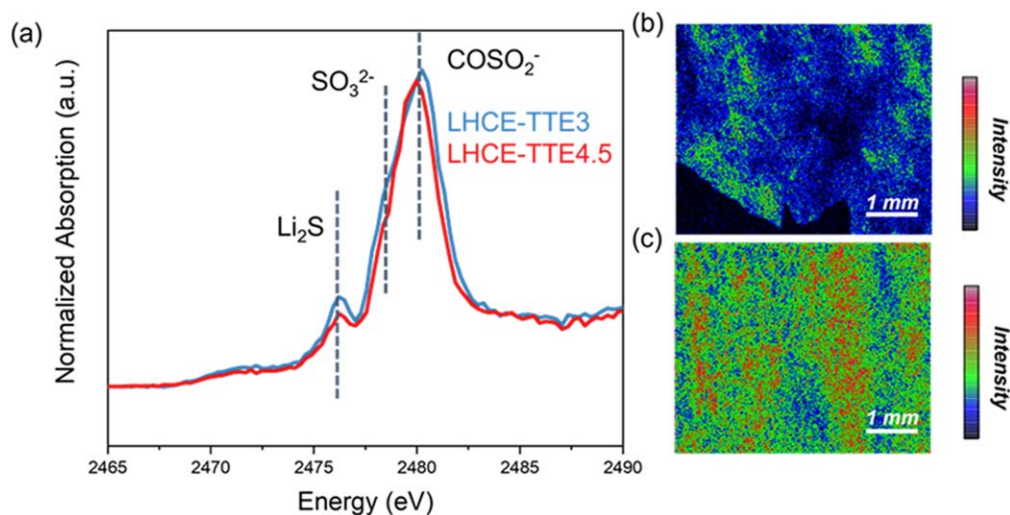


**Figure 4.** (a) Sulfur K-edge X-ray absorption spectroscopy (XAS) of Cu foil with deposited lithium in Li/Cu cells. X-ray fluorescence images of sulfur species on Cu foil collected at 2482 eV using (b) LHCE-TTE3 and (c) LHCE-TTE4.5.

TTE4.5, the reduction of FEC additive generated a LiF-rich SEI, with more FSI<sup>-</sup> derived sulfur species accumulated in the outer

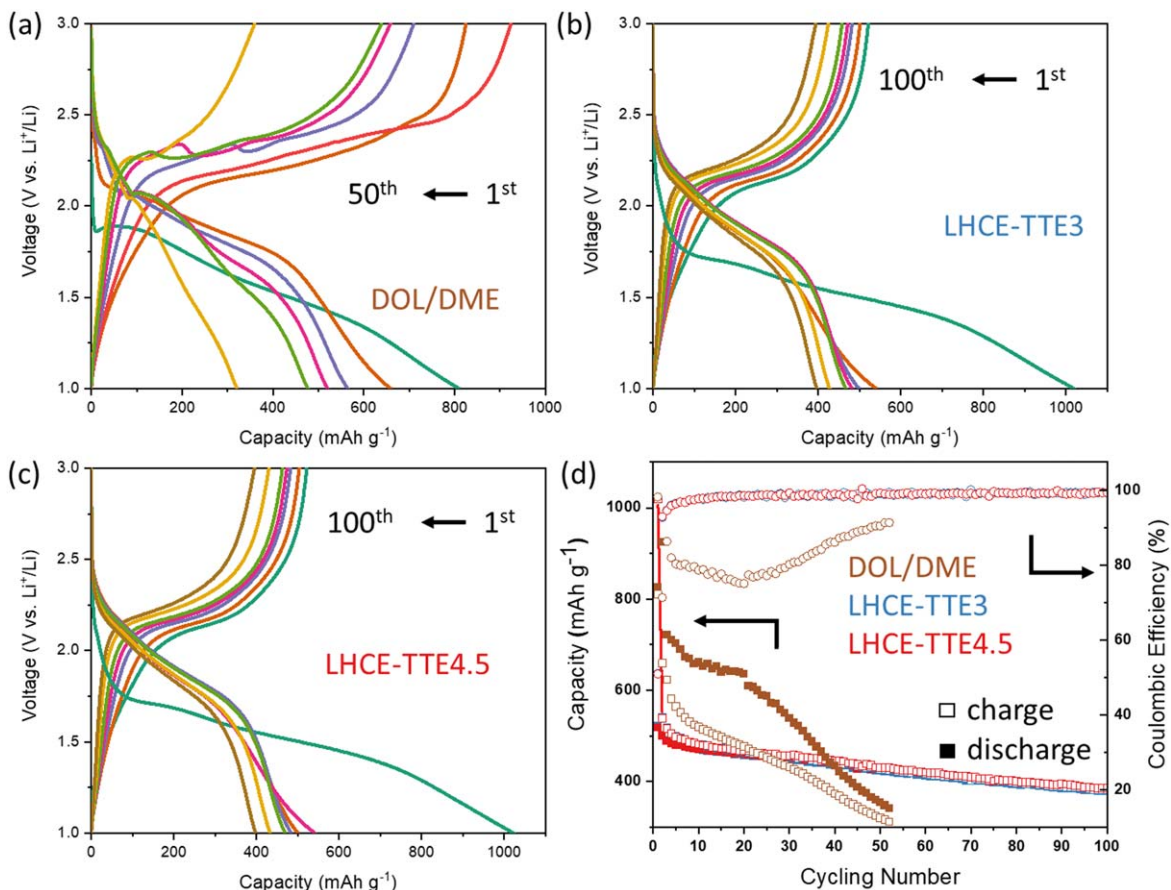


**Figure 5.** Room temperature charge/discharge curves of Li/SPAN cells using (a) 1 M LiTFSI in DOL/DME; (b) LHCE-TTE3; and (c) LHCE-TTE4.5 electrolytes; (d) long-term capacity retention and coulombic efficiency of Li/SPAN cells.

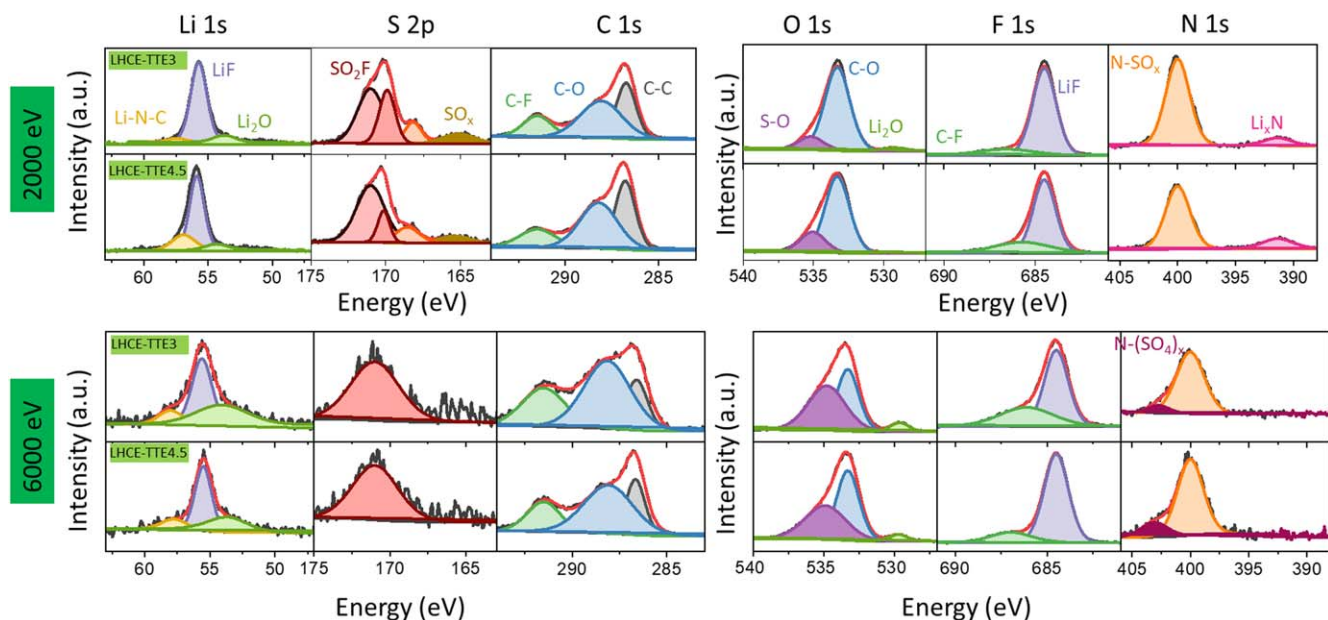


**Figure 6.** XPS spectra of Li foil harvested from cycled Li/SPAN cells using LHCE-TTE3 and LHCE-TTE4.5 measured at different photon energy.

layer, and  $\text{Li}_2\text{O}$  in the bottom layer, forming a hierarchical SEI, providing robust Li metal passivation. Interestingly, although the electrochemical performance differences between these two LHCEs were not significant at room temperature, the electrochemical

performances of LHCE-TTE3 and LHCE-TTE4.5 are quite different at low temperatures, as shown in Fig. 7.

Taking advantage of the high ionic conductivity of IZ-based electrolytes at low temperature as reported in our previous work,<sup>12,13</sup> low-temperature performance of Li/SPAN cell was further studied.

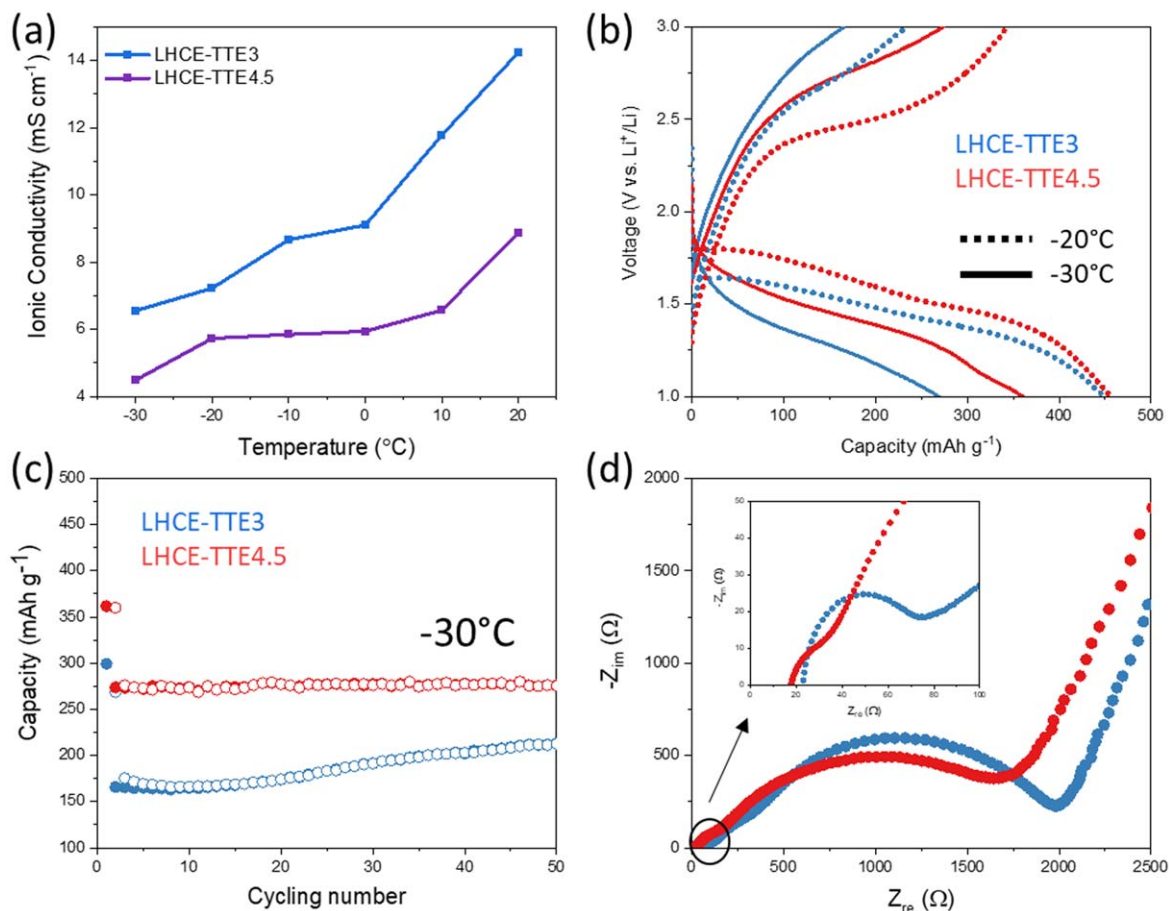


**Figure 7.** (a) ionic conductivity of LHCE-TTE3 and LHCE-TTE4.5. (b) Charge-discharge voltage profile of Li/SPAN cells at  $-20\text{ }^{\circ}\text{C}$  (dot line) and  $-30\text{ }^{\circ}\text{C}$  (solid line) using LHCE-TTE3 (blue) and LHCE-TTE4.5 (red). (c) Li-SPAN cycling stability at  $-30\text{ }^{\circ}\text{C}$  using LHCE-TTE3 (blue) and LHCE-TTE4.5 (red). (d) EIS results of Li/SPAN cells after 50 cycles at  $-30\text{ }^{\circ}\text{C}$ .

Due to the high viscosity of TTE diluent (1.43 cP at  $25\text{ }^{\circ}\text{C}$ ),<sup>18</sup> lower ionic conductivity was observed in the LHCE-TTE4.5 electrolyte, which has a higher ratio of TTE, as shown in Fig. 7a. However, it is quite interesting to note that the relatively lower bulk ionic conductivity does not necessarily translate to worse electrochemical performance at low temperature, as reported in the literature.<sup>23</sup> As pointed out in previous studies, it is the SEI impedance, not the bulk electrolyte conductivity, plays the dominating role for electrochemical performance at low temperature.<sup>24,25</sup> Figure 7b shows the first cycle charge/discharge profile of the Li/SPAN cells at low temperature. Higher reversible capacity was delivered when using LHCE-TTE4.5 at  $-20\text{ }^{\circ}\text{C}$  ( $340.7\text{ mAh g}^{-1}$ ) and  $-30\text{ }^{\circ}\text{C}$  ( $273.8\text{ mAh g}^{-1}$ ), when compared with that using LHCE-TTE3 at  $-20\text{ }^{\circ}\text{C}$  ( $231.0\text{ mAh g}^{-1}$ ) and  $-30\text{ }^{\circ}\text{C}$  ( $165.4\text{ mAh g}^{-1}$ ). This trend was further supported by the low-temperature long-term cycling (Fig. 7c), in which LHCE-TTE4.5 delivered higher capacity with superior capacity retention. Impedance analysis was carried out on the cells after 50 cycles at  $-30\text{ }^{\circ}\text{C}$  to understand the stability of interphase. As shown in Fig. 7d, the charge transfer resistance ( $R_{ct}$ ) after cycling in LHCE-TTE3 is higher than that of LHCE-TTE4.5. Also, the SEI impedance ( $R_{SEI}$ ) of LHCE-TTE3 is almost three times higher than that of LHCE-TTE4.5, which is a critical factor that led to a faster capacity decay. These results show that the advantages of a better SEI formed in LHCE-TTE4.5 can be demonstrated more clearly at low-temperature operations. The more stable SEI with lower impedance could suppress undesirable side reactions more effectively, facilitate faster ion transportation, and enable low-temperature electrochemical performance for Li/SPAN cells. Therefore, the better SEI formed in LHCE-TTE4.5 played a critical role for the better low-temperature performance, regardless of the slightly lower ionic

conductivity in the bulk electrolyte of LHCE-TTE4.5 than LHCE-TTE3. The performance difference between LHCE-TTE3 and LHCE-TTE4.5 is negligible at room temperature (Fig. 5) but quite significant at low temperature (Fig. 7). We have tried to use these IZ-based electrolytes for full cells using transition metal oxide cathodes to improve their low-temperature performance. Unfortunately, the results were not satisfactory, mainly because the oxidation stability of IZ-based electrolytes at high operating voltage is not good enough.

## Conclusions

In summary, isoxazole-based electrolytes have been developed, and their application for lithium metal batteries has been investigated. Isoxazole-based localized high concentration electrolytes (LHCEs) with FEC additive can significantly enhance the stability and functionality of SEI, and high Coulombic efficiency (CE) of 98.6% was achieved, benefitted from the FSI<sup>-</sup> and FEC derived better SEI with LiF and sulfur-rich components. With a lower isoxazole/TTE volume ratio in LHCE-TTE4.5, better SEI was formed, resulting in a superior electrochemical performance at low temperature. The Li/SPAN cell using LHCE-TTE4.5 delivered  $340.7\text{ mAh g}^{-1}$  at  $-20\text{ }^{\circ}\text{C}$  and  $273.8\text{ mAh g}^{-1}$  at  $-30\text{ }^{\circ}\text{C}$ , with 99.85% capacity retention after 50 cycles at  $-30\text{ }^{\circ}\text{C}$ . This work demonstrated the importance of SEI for low-temperature applications. Compared with the bulk ionic conductivity of electrolyte, the stability and impedance of the SEI have a significantly greater impact on the electrochemical performance at low temperatures. These results provide valuable information for developing and screening new electrolytes for low-temperature applications.

### Disclaimer

Commercial equipment is identified in this report in order to specify the experimental procedure adequately and does not imply recommendation or endorsement by the National Institute of Standards and Technology, nor is it intended to imply that the equipment identified is necessarily the best available for the purpose.

### Acknowledgments

The work done at Brookhaven National Laboratory was supported by the Assistant Secretary for Energy Efficiency and Renewable Energy, Vehicle Technology Office of the US Department of Energy (DOE) through the Advanced Battery Materials Research (BMR) Program, including Battery500 Consortium under contract no. DE-SC0012704. This work at University of California San Diego was supported by the Office of Vehicle Technologies of the U.S. Department of Energy through the Advanced Battery Materials Research (BMR) Program (Battery500 Consortium) under Contract no. DE-EE0007764. This research used beamline 8-BM (TES) and 7-ID-2 (SST-2) of the National Synchrotron Light Source II, U.S. DOE Office of Science User Facilities, operated for the DOE Office of Science by Brookhaven National Laboratory under contract no. DE-SC0012704. SEM measurements for this manuscript were performed at Center for Functional Nanomaterials, a U.S. DOE office of Science User Facility, at Brookhaven National Laboratory under the contract no. DE-SC0012704. Prof. S. Whittingham is supported by the Assistant Secretary for Energy Efficiency and Renewable Energy, Vehicle Technology Office of the U.S. DOE through the Advanced Battery Materials Research (BMR) Program, including Battery500 Consortium under contract No. DE-EE0007765.

### ORCID

Seong-Min Bak  <https://orcid.org/0000-0002-1626-5949>

Ping Liu  <https://orcid.org/0000-0002-1488-1668>

Xiao-Qing Yang  <https://orcid.org/0000-0002-3625-3478>

### References

1. S. S. Zhang, K. Xu, and T. R. Jow, *Electrochim. Acta*, **49**, 1057 (2004).
2. K. Xu, *Chem. Rev.*, **114**, 11503 (2014).
3. Q. Li, J. Chen, L. Fan, X. Kong, and Y. Lu, *Green Energy & Environment*, **1**, 18 (2016).
4. M. Marcinek et al., *Solid State Ionics*, **276**, 107 (2015).
5. K. Xu, *Chem. Rev.*, **104**, 4303 (2004).
6. C. Wang, Y. S. Meng, and K. Xu, *J. Electrochem. Soc.*, **166**, A5184 (2019).
7. H. Zhang, G. G. Eshetu, X. Judez, C. Li, L. M. Rodriguez-Martinez, and M. Armand, *Angew. Chem. Int. Ed.*, **57**, 15002 (2018).
8. K. Kim, H. Ma, S. Park, and N.-S. Choi, *ACS Energy Lett.*, **5**, 1537 (2020).
9. X. Cao, H. Jia, W. Xu, and J.-G. Zhang, *J. Electrochem. Soc.*, **168**, 010522 (2021).
10. J. G. Zhang, W. Xu, J. Xiao, X. Cao, and J. Liu, *Chem. Rev.*, **120**, 13312 (2020).
11. J. Qian, W. A. Henderson, W. Xu, P. Bhattacharya, M. Engelhard, O. Borodin, and J.-G. Zhang, *Nat. Commun.*, **6**, 6362 (2015).
12. S. Tan, U. N. D. Rodrigo, Z. Shadike, B. Lucht, K. Xu, C. Wang, X. Q. Yang, and E. Hu, *ACS Appl. Mater. Interfaces*, **13**, 24995 (2021).
13. N. D. Rodrigo, S. Tan, Z. Shadike, E. Hu, X.-Q. Yang, and B. L. Lucht, *J. Electrochem. Soc.*, **168**, 070527 (2021).
14. J. Holoubek et al., *Nat. Energy*, **6**, 303 (2021).
15. B. D. Adams, J. Zheng, X. Ren, W. Xu, and J.-G. Zhang, *Adv. Energy Mater.*, **8**, 1702097 (2018).
16. T. T. Hagos et al., *ACS Appl. Mater. Interfaces*, **11**, 9955 (2019).
17. X. Cao et al., *Nat. Energy*, **4**, 796 (2019).
18. X. Cao et al., *Proc Natl Acad Sci U S A*, **118**, e2020357118 (2021).
19. X. Ren et al., *Chem*, **4**, 1877 (2018).
20. C. Fiedler, B. Luerksen, M. Rohnke, J. Sann, and J. Janek, *J. Electrochem. Soc.*, **164**, A3742 (2017).
21. M. R. Busche, M. Weiss, T. Leichtweiss, C. Fiedler, T. Drossel, M. Geiss, A. Kronenberger, D. A. Weber, and J. Janek, *Adv. Mater. Interfaces*, **7**, 2000380 (2020).
22. X. Xing, Y. Li, X. Wang, V. Petrova, H. Liu, and P. Liu, *Energy Storage Mater.*, **21**, 474 (2019).
23. X. Zhang et al., *Adv. Energy Mater.*, **10**, 2000368 (2020).
24. S. S. Zhang, *ChemElectroChem*, **7**, 3569 (2020).
25. K. X. S. S. Zhang and T. R. Jow, *Electrochem. Commun.*, **4**, 928 (2002).